J Mater Sci: Mater Electron (2016) 27:6419–6424
DOI 10.1007/s10854-016-4580-8

Abnormal resistivity-temperature characteristic in fluorite type Bi/K-substituted ceria ceramics

Junke Wang[1] · Hong Zhang[1,3] · Zhiyuan Ma[1] · Yu Zhang[1] · Zhicheng Li[1,2]

Received: 17 December 2015 / Accepted: 23 February 2016 / Published online: 5 March 2016

Abstract Bi/K-substituted CeO_2 ($Bi_xK_yCeO_{2+\delta}$, x and y are 0.2 or 0.3) ceramics were prepared by a wet chemical route. The $Bi_xK_yCeO_{2+\delta}$ ceramics have cubic fluorite crystalline structure and show an abnormal resistivity-temperature characteristic in which the resistivities increase sharply at 150−190 °C. In situ XRD investigations revealed that the $Bi_{0.3}K_{0.2}CeO_{2.55}$ ceramic maintained the cubic fluorite structure and did not show any detectable phase transition excepting the lattice parameters increased during heating from 25 to 220 °C. The complex impedance and electrical modulus analysis were performed to reveal the abnormal resistivity-temperature effect. The electrical properties are attributed to the grain effect instead of the grain-boundary effect. The abnormal resistivity-temperature characteristic was proposed to originate from the transition of conduction models from a long-range conduction to a localized conduction.

1 Introduction

Electronic materials with the resistivity-temperature sensitivity are always attracted much attention for their unique functional applications such as sensors and actuators, temperature controller, self-controlled heating element and overload protector, etc. Among various resistivity-temperature sensitive resistors (i.e., thermistors), the ones showing a positive temperature coefficient (PTC) or negative temperature coefficient (NTC) effect are extensively applied in industrial and domestic devices for the temperature measurement, automatic control, temperature compensation and voltage stabilization, owing to their high sensitivity and reliability. Meanwhile, the transition metal oxides such as VO_2 and V_2O_3 with the metal–insulator transition feature are also of interest in practical applications and theoretical research [1–5]. In the traditional PTC ceramic thermistors, $BaTiO_3$-based compounds are the most important ones for the practical applications [6–8]. To get the Curie temperatures higher than 120 °C, lead (Pb) is used to substitute into the $BaTiO_3$ to form the $(Ba,Pb)TiO_3$ ceramics. However, due to the environmental pollution of Pb-contained compounds, the $(Ba,Pb)TiO_3$-based products are going to be prohibited in the electric devices. Some new types of lead-free PTC materials such as $BaTiO_3$-$(Bi_{1/2}Na_{1/2})TiO_3$ and $BaTiO_3$-$(Bi_{1/2}K_{1/2})TiO_3$ systems have been developed in past decade [9–11]. The related PTC conduction mechanisms were found to follow the Heywang–Jonker model, in which the grain boundary effect plays a key role in the resistivity jump around the Curie temperatures, as shown in the $BaTiO_3$-based thermistors [6–8].

On the other hand, CeO_2-based materials have been widely studied for their applications in oxygen ionic conductors as an alternative to Y_2O_3-stabilized ZrO_2 for their high ionic conductivity [12–16]. The CeO_2-based oxygen ionic conductors present a nearly linear relationship between temperature (1/T) and conductivity ($\ln \sigma$), followed the Arrhenius equation, in a wide temperature range. As far as we know, there has been no report on the characteristic of temperature dependence of electronic

✉ Zhicheng Li
zhchli@csu.edu.cn

[1] School of Materials Science and Engineering, Central South University, Changsha 410083, China

[2] State Key Laboratory of Powder Metallurgy, Central South University, Changsha 410083, China

[3] Institute for Materials Microstructure, Central South University, Changsha 410083, China

resistivity such as the PTC effect in the fluorite CeO_2-based ceramics so far.

In present work, new compounds of Bi/K-substituted CeO_2 ($Bi_xK_yCeO_{2+\delta}$, denoted as BKC, where $x = 0.2$ or 0.3, $y = 0.2$ or 0.3, and δ is the increased oxygen atomic number for the Bi/K substitution) is developed and the related temperature dependence of electronic conductivity is investigated. It was found that the BKC ceramics display an abnormal resistivity-temperature characteristic, i.e., an excellent PTC effect, with the resistivities jump up at 150−190 °C. The possible PTC mechanisms were studied by analyzing the complex impedance spectra, and were revealed not to follow the conventional Heywang−Jonker model as that in the $BaTiO_3$-based thermistors.

2 Experimental procedure

The BKC materials were prepared by using a wet chemical route. Appropriate amount of Bi_2O_3, K_2CO_3 and CeO_2 were weighed according to the formula of $Bi_xK_yCeO_{2+\delta}$ ($x = 0.2$ or 0.3, $y = 0.2$ or 0.3). CeO_2 was dissolved into a solution of H_2O_2 and HNO_3 in distilled water, while Bi_2O_3 and K_2CO_3 were dissolved together into dilute nitric acid. Then the two solutions were mixed together, and the pH value of the mixture was adjusted to about 8 by dropping dilute ammonium hydroxide. The mixture was heated with stirring to get the dried precursors. The BKC powders were obtained by calcining the precursors at 750 °C for 5 h. The BKC powders were pressed into pellets with diameter of 10 mm and thickness of about 3 mm, and the pellets were sintered in air at 800 °C for 10 h. The sintered ceramics were ground to about 1 mm in thickness. Silver paste was painted on both sides of the ceramics and was heated to 550 °C for 5 min to obtain the ohmic electrodes.

The crystalline phase of the calcined powders and as-sintered ceramics were identified by X-ray diffraction (XRD, Rigaku D/max 2500, Japan) with CuK_α radiation ($\lambda = 0.154056$ nm). In situ XRD investigations of a BKC ceramic were performed to identify the phase component and possible phase transition by heating the sample from 25 to 220 °C. The direct-current (DC) temperature dependence of resistance of the BKC ceramics was characterized by using a resistance-temperature measurement system (ZWX-C, China). Alternating current (AC) impedance measurements were performed by using an electrochemical measurement system (Gamry Reference 600, USA) over the frequency range 1 Hz to 1 MHz, in the temperature range of 25−200 °C. Transmission electron microscopy (TEM, Tecnai G^2 F20, FEI) and scanning electron microscopy (FESEM, Quanta FEG 250, USA) were used to investigate the morphology and microstructure of the samples.

3 Results & discussion

3.1 Phases and electrical properties

Figure 1a shows XRD patterns of the as-sintered BKC ceramics measured at room temperature. The diffraction peaks are in accordance with the ones of a cubic fluorite structure CeO_2 (ICCD No. 34-0394, space group of $Fm\bar{3}m$) excepting for two minor secondary phases that emerge at the angles $2\theta = 26.94°$ and 27.42°, respectively. The impurity phases were identified to be monoclinic Bi_2O_4 (ICCD No. 50-0864, space group of C2/c) at $2\theta = 26.94°$ and cubic Bi_2O_3 (ICCD No. 77-0374, space group of $Fm\bar{3}m$) at $2\theta = 27.42°$. The diffraction peaks for the BKC cubic fluorite phase shifted to higher diffraction angles in comparison with those of pure CeO_2 (ICCD No. 34-0394, $a = 0.5411$ nm), indicating that the lattice parameter of the BKC ceramic (e.g., $a = 0.5401$ nm for $Bi_{0.3}K_{0.2}CeO_{2.55}$) decreased for the Bi/K substitution. For these cases, it is demonstrated that K^+ and most of Bi^{3+} ions had formed a solid solution with CeO_2. Figure 1b shows a TEM analysis of a $Bi_{0.3}K_{0.2}CeO_{2.55}$ ceramic, the particles are uniformed in size with an average diameter of about 100 nm. The insert selected area electron diffraction (SAED) pattern reveals that the BKC has a cubic fluorite crystal structure, which is consistent with the XRD results. Figures 1c, d shows the SEM images of the fracture surface of a $Bi_{0.3}K_{0.2}CeO_{2.55}$ ceramic. There are not obvious gas pores and the grains bind good each other, indicating the ceramic has good sintering state.

As analyzed in Fig. 1a, the lattice parameters of BKC are less than that of pure CeO_2 crystal, although the K^+ ion has a larger ionic radius (1.51 Å) than that of Ce^{4+} ion (1.11 Å), while Bi^{3+} ion has the same ionic radius of 1.11 Å at 8-coordination status. It should be attributed to the formation of oxygen vacancies when K^+ and Bi^{3+} substituted into the CeO_2 crystalline lattice, the corresponding defect reactions can be described with the Kröger–Vink type equations:

$$K_2O \xrightarrow{CeO_2} 2K'''_{Ce} + O_O + 3V^{\cdot\cdot}_O \quad (1)$$

$$Bi_2O_3 \xrightarrow{CeO_2} 2Bi'_{Ce} + 3O_O + V^{\cdot\cdot}_O \quad (2)$$

Figure 2a shows the temperature dependence of electrical resistivity by DC measurement for the BKC ceramics. One can see that all the BKC ceramics show the typical effect PTC of resistivity as that of the traditional $BaTiO_3$-based PTC ceramics. For example, the $Bi_{0.3}K_{0.2}CeO_{2.55}$ ceramic has a room temperature resistivity (ρ_{25}) of 4.68×10^4 Ω cm, and possesses a resistivity jump of $\rho_{max}/\rho_{min} = 1.11 \times 10^3$ taken place at around 180 °C. The PTC

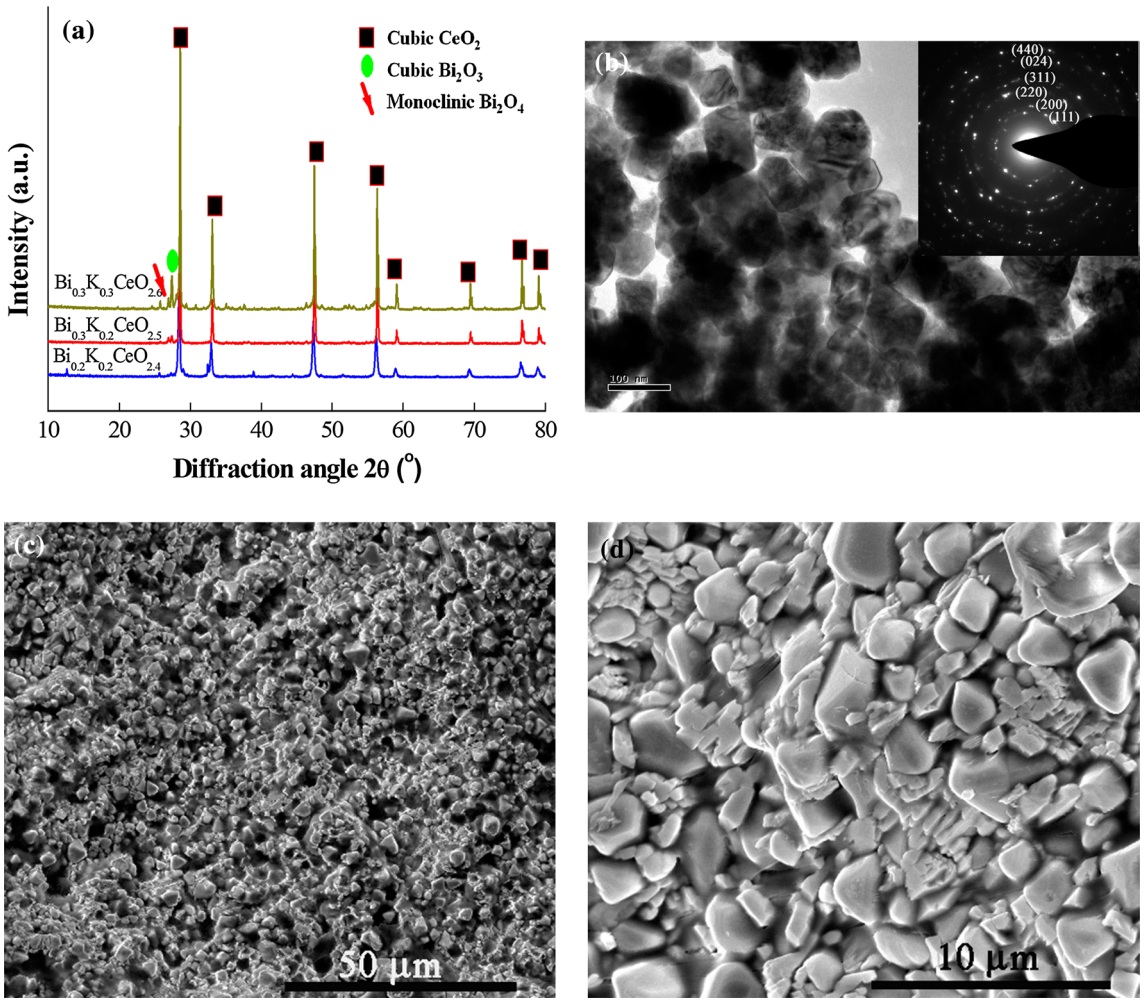

Fig. 1 Phase and microstructure analysis of the as-sintered BKC ceramic, showing that the ceramic consists of the cubic fluorite phase, **a** XRD patterns measured at room temperature, **b** TEM image and related electron diffraction pattern of $Bi_{0.3}K_{0.2}CeO_{2.55}$ sample, **c**, **d** SEM images of fracture surface of $Bi_{0.3}K_{0.2}CeO_{2.55}$ ceramic

effect is comparable with the ones of the $BaTiO_3$-based ceramics.

The $BaTiO_3$-based ceramics have typical phase transformation from the tetragonal ferroelectric phase to the cubic paraelectric phase at temperature around its Curie point when the temperature increases [17]. To investigate the phase component and possible phase transition in the BKC ceramics during the heating process, in situ XRD measurements with a $Bi_{0.3}K_{0.2}CeO_{2.55}$ ceramic were employed in the temperature range from 25 to 220 °C. The in situ XRD results are shown in Fig. 2b. At each measurement temperature, the BKC ceramic remains the same cubic fluorite structure as those discussed in Fig. 1a, indicating there is no phase transition taken place during the temperature rising. These also indicate that the abnormal temperature dependence of resistivity does not result from the tetragonal-cubic transformation characteristic as that in $BaTiO_3$-based ceramics.

In addition, as shown in Fig. 2b, the diffraction peaks shift towards lower diffraction angles with the rising temperatures, meaning that the lattice parameters of the BKC ceramic increased. The BKC lattice parameters at various temperatures were refined by using the Jade 6 + pdf2003 soft and the results are shown in Fig. 2c. The lattice parameter increased slightly with the temperature increased in the low temperature region (<180 °C), but obviously increased when the temperatures higher than 180 °C, e.g., the lattice parameter increased from 0.5401 nm (180 °C) to 0.5427 nm (190 °C) and 0.5455 nm (200 °C). It should be noted that the lattice parameter jump and the resistivity jump took place at the similar temperature region.

3.2 Impedance analysis

In order to investigate the conduction characteristic in the BKC ceramics, AC impedance were employed and

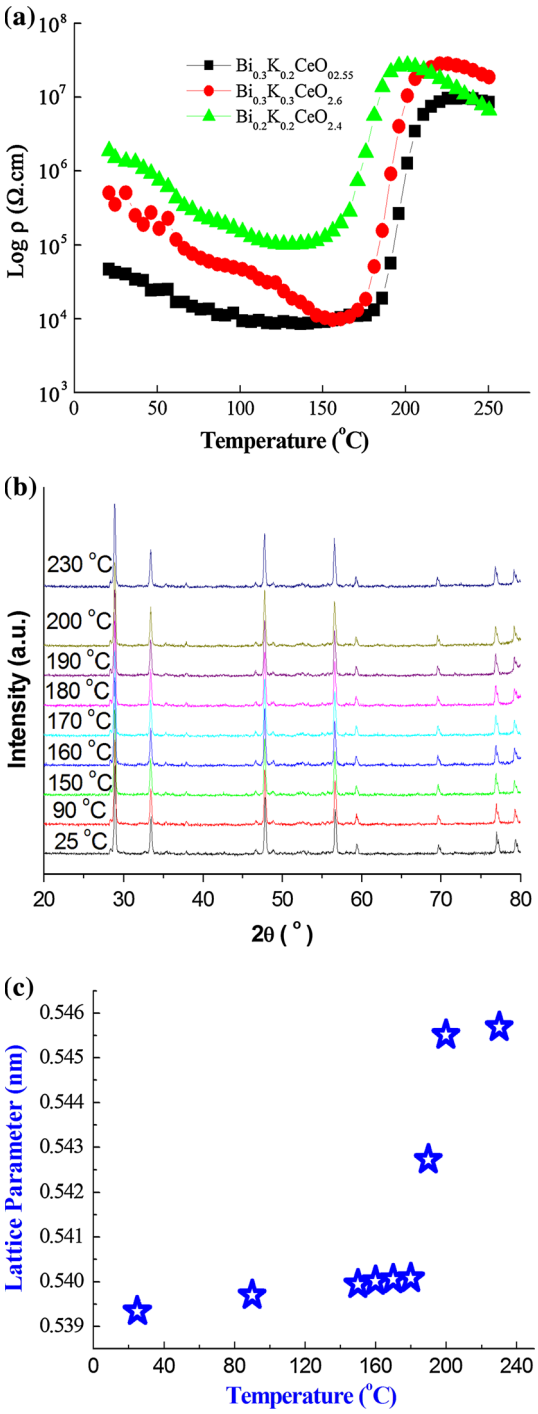

Fig. 2 Temperature dependence of the properties of BKC ceramic, **a** resistivity-temperature characteristic, showing an abnormal resistivity jump at temperatures region between 150 and 200 180 °C, **b** in situ XRD patterns of $Bi_{0.3}K_{0.2}CeO_{2.55}$ ceramic, revealing the ceramic remains cubic fluorite lattice during the temperature rising, **c** lattice parameter versus temperature based on (**b**) measurements, showing obvious change in lattice parameter around 180 °C

analyzed in a $Bi_{0.3}K_{0.2}CeO_{2.55}$ ceramic. Figure 3 shows the Cole–Cole plots of the complex impedance spectra of the BKC ceramic measured at 25, 60, 120, 160, 180 and

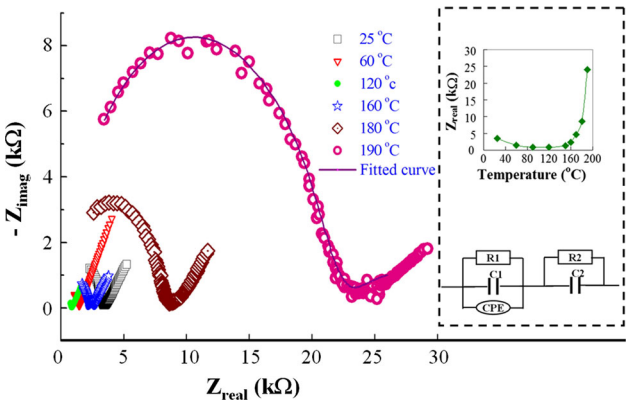

Fig. 3 Complex impedance analysis of $Bi_{0.3}K_{0.2}CeO_{2.55}$ ceramic measured at 25, 60, 120, 160, 180 and 190 °C, respectively. The *upper-right inset* shows the temperature dependence of resistivity from grain effect, and the *down-right inset* is an equivalent circuit for impedance data fitting

190 °C, respectively. A solid line representing a fitted curve derived from the equivalent circuit (down-right inset in Fig. 3) is shown at the 190 °C plot. Where, *R* represents the resistance of the ceramic, *C* represents capacitance, *CPE* are a constant phase element which is caused by interior structure inhomogeneity or uncertain defects. It can be seen that the fitted curve is in good accordance with the measured data (open circles). The other measurement plots were also fitted by using the equivalent circuit, but not shown here. Each of the impedance spectra, as shown in Fig. 3, consists of two parts of conduction components: higher-frequency region (left part spectrum) from the grain effect (bulk effect) and lower-frequency region (right part, oblique line) from the electrode polarization for the possible ionic conduction (e.g. oxygen ionic transition).

When the temperature rises, the bulk-effect arcs become smaller at first, and then change to obviously larger at above 180 °C (the related real part impedance from the bulk effect are shown in the upper-right inset in Fig. 3). The temperature dependence of impedance from grain effect is in agreement with the one of the AC resistance in BKC ceramic as shown in Fig. 2a. These indicate that the grain effect makes a main contribution to the PTC characteristic of the BKC ceramics. The PTC mechanism is obviously different from the one of the perovskite $BaTiO_3$-based ceramics, in which the grain-boundary effect acts as the key role in the PTC effect.

To further reveal the PTC effect in the BKC ceramics, the frequency dependence of imaginary impedance Z'' and electrical modulus M'' was discussed with a $Bi_{0.3}K_{0.2}CeO_{2.55}$ ceramic. Figure 4a shows the plots of frequency dependence of Z'' measured at 25, 160, 180 and 190 °C, respectively. Each plot displays one peak in the high-frequency region. Where, the impedance peak Z''_{max} at 160 °C is lower than that at 25 °C, but the ones at 180 and 190 °C

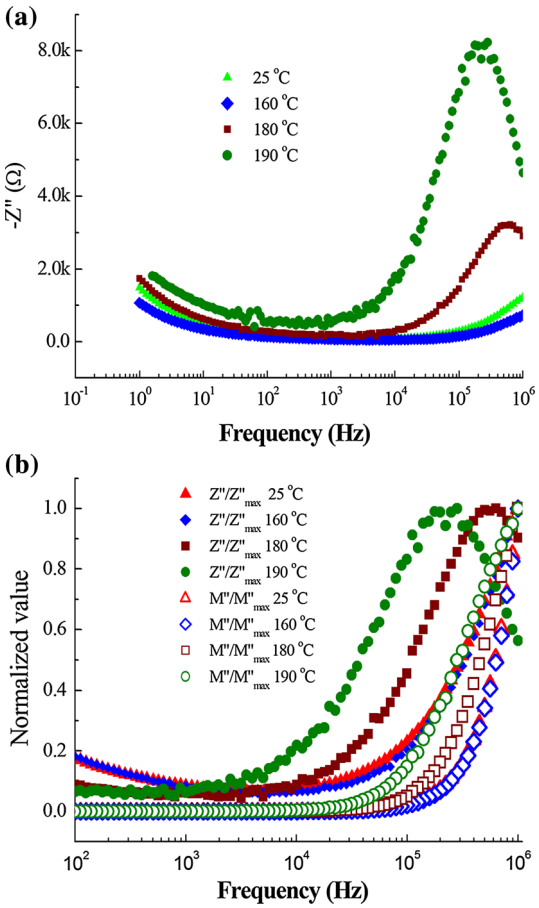

Fig. 4 Frequency dependence of imaginary impedance Z'' and electrical modulus M'' of $Bi_{0.3}K_{0.2}CeO_{2.55}$ ceramic, **a** Z''-frequency plots, **b** Z''/Z''_{max} and M''/M''_{max} as a function of frequency at 25, 160, 180 and 190 °C, respectively

are higher than that at 25 °C. According to the study by Chatterjee et al. [18], the peak value Z''_{max} is proportional to the grain resistance R_g as represented by Eq. (3).

$$Z''_{\max} = R_g\left[\frac{\omega\tau}{1+\omega^2\tau^2}\right] \tag{3}$$

where ω is the angular frequency, and τ is the conductivity relaxation time $\tau = RC$ [19]. These reveal that the τ increases obviously around 180 °C during the temperature rising. The increase in relaxation time can also be due to the increase in effective dielectric constant. Accordingly, the mobility of electron decreased and a localized conduction state formed at temperatures higher than 180 °C, resulting in the sharp increase of the grain-effect resistivity [20].

Figure 4b shows the frequency dependence of normalized values, Z''/Z''_{max} and M''/M''_{max}, at 25, 160, 180 and 190 °C, respectively, in $Bi_{0.3}K_{0.2}CeO_{2.55}$ ceramic. The Z''/Z''_{max} and M''/M''_{max} peaks locate almost the same frequencies at 25 and 160 °C, respectively, indicating the existence of long-range conduction at temperatures lower than 160 °C [21]. The Z''/Z''_{max} peaks shift obviously toward the lower frequency regions when the temperature increases at 180 °C and higher, and the frequency difference between the Z''/Z''_{max} and M''/M''_{max} peaks become larger, indicating that the conduction model transformed from the long-range conduction to the so-called localized conduction [19].

As shown in Eqs. (1) and (2), the dissociation/association reactions between the substitution defect and vacancy in the Bi/K-substituted CeO_2 can be illustrated as Eqs. (4) and (5), respectively.

$$Bi'_{Ce} + V^{\cdot\cdot}_{O} \Leftrightarrow (Bi'_{Ce}V^{\cdot\cdot}_{O}) \tag{4}$$

$$K'''_{Ce} + V^{\cdot\cdot}_{O} \Leftrightarrow (K'''_{Ce}V^{\cdot\cdot}_{O}) \tag{5}$$

The dissociation/association reactions might strongly influence elastic property and formed the so-called "chemical strain" effect [17, 22–24]. At room temperature, the cations and anions shift with respect to each other so that Ce^{4+} ions might shift away from the oxygen vacancies, locally distorting the lattice symmetry [25]. High temperature reduces the repulsion inside the dissociation/association complexes, increasing the lattice parameter. The dissociation of the associated defects becomes stronger when the temperature increases. The defect dissociation took place rapidly above 150 °C, deriving the fact that the values for the lattice parameter of Gd-doped ceria exhibited large variations [24]. Similarly, in the Bi/K-substituted CeO_2, the related dissociation reactions might be accompanied by the ionic displacement polarization, resulting in the increase of dielectricity and electrical resistance increase.

Based on the above discussion, the PTC effect in a BKC ceramic should result from the long-range conduction to localization conduction around the resistivity-jump temperature (T_c). Below the T_c, the long-range conduction acts as the main role depending on the transport of charge carriers induced by the doping of Bi^{3+} and K^+, resulting in a low resistivity. During the temperature rising, the lattice parameter of the BKC ceramic increases, the associated defect complexes dissociates, and the resistivity jump takes place around the T_c. It is in agreement with the suggestion by Imada et al. [21], there should be a threshold value for the lattice parameters to keep a suitable atomic distance in the ceramic, beyond which the difficulty for the migration of charge carriers is enhanced, resulting in the ceramic resistivity jumps.

4 Conclusions

The fluorite BKC ceramics ($Bi_xK_yCeO_{2+\delta}$, $x = 0.2$ or 0.3, $y = 0.2$ or 0.3) display unique PTC effect with the resistivity jump temperatures around 150−190 °C. The in situ

XRD investigations reveal that there is no detectable phase transition in the $Bi_xK_yCeO_{2+\delta}$ ceramics during the heating process, and the lattice parameter increases obviously around the resistivity-jump temperature. The impedance and modulus analysis reveal that the main contribution to the PTC effect is derived from grain effect instead of grain-boundary effect. The PTC mechanism in the $Bi_xK_yCeO_{2+\delta}$ ceramics is different from that in the perovskite $BaTiO_3$-based ceramics. The origin of the PTC effect is supposed to be the change of conductive models from the long-range conduction to the localized conduction, for the association and dissociation of defect complexes, around the resistivity-jump temperature.

Acknowledgments The authors acknowledge the support of the National Nature Science Foundation of China (No. 51172287) and the Laboratory Research Fund by the State Key Laboratory of Powder Metallurgy, Central South University, China.

References

1. P. Pfalzer, G. Obermeier, M. Klemm, S. Horn, M.L. denBoer, Phys. Rev. B **73**, 144106 (2006)
2. N. Li, M. Hu, J.R. Liang, X. Liu, M.J. Wu, J. Mater. Sci. Mater. Electron. **26**, 6920–6925 (2015)
3. T.H. Yang, R. Aggarwal, A. Gupta, H. Zhou, R.J. Narayan, J. Narayan, J. Appl. Phys. **107**, 053514 (2010)
4. T. Mizokawa, Nat. Phys. **9**, 612–613 (2013)
5. N.B. Aetukuri, A.X. Gray, M. Drouard et al., Nat. Phys. **9**, 661–666 (2013)
6. M. Yuasa, T. Nagano, N. Tachibana, T. Kida, K. Shimanoe, J. Am. Ceram. Soc. **96**, 1789–1794 (2013)
7. Y.X. Hu, T. Wen, Q.Y. Fu, D.X. Zhou, Z.P. Zheng, W. Luo, J. Zhao, J. Mater. Sci. Mater. Electron. **26**, 7784–7789 (2015)
8. Z.C. Li, B. Bergman, Ceram. Int. **31**, 375–378 (2005)
9. S. Leng, G. Li, L. Zheng, W. Shi, Y. Zhu, J. Mater. Sci. Mater. Electron. **24**, 431–435 (2013)
10. P.H. Xiang, H. Takeda, T. Shiosaki, J. Appl. Phys. **103**, 064102 (2008)
11. J. Zhao, Y. Pu, Y. Wu, P. Zhang, J. Mater. Sci. Mater. Electron. **26**, 6051–6056 (2015)
12. J.V. Herle, T. Horita, T. Kawada, N. Sakai, H. Yokokawa, M. Dokiya, J. Am. Ceram. Soc. **80**, 933–940 (1997)
13. S.S. Bhella, L.M. Kuti, Q. Li, V. Thangadurai, Dalton Trans. **43**, 9520–9528 (2009)
14. Z. Gao, X. Liu, B. Bergman, Z. Zhao, J. Power Sources **208**, 225–231 (2012)
15. Z. Li, H. Zhang, B. Bergman, Ceram. Int. **34**, 1949–1953 (2008)
16. M. Prekajski, Z. Dohčević-Mitrović, M. Radović et al., J. Eur. Ceram. Soc. **32**, 1983–1987 (2012)
17. W. Heywang, J. Mater. Sci. **6**, 1214–1224 (1971)
18. S. Chatterjee, P.K. Mahapatra, R.N.P. Choudhary, A.K. Thakur, Phys. Status Solidi (a) **201**, 588–595 (2004)
19. R. Gerhardt, J. Phys. Chem. Solids **55**, 1491–1506 (1994)
20. R. Ranjian, R. Kumar, B. Behera, R.N.P. Choudhary, Phys. B **404**, 3709–3716 (2009)
21. M. Imada, A. Fujimori, Y. Tokura, Rev. Mod. Phys. **70**, 1039–1263 (1998)
22. A. Atkinson, Solid State Ionics **95**, 249–258 (1997)
23. M. Greenberg, E. Wachtel, I. Lubomirsky, J. Fleig, J. Maier, Adv. Funct. Mater. **16**, 48–52 (2006)
24. A. Kossoy, Y. Feldman, E. Wachtel, I. Lubomirsky, J. Maier, Adv. Funct. Mater. **17**, 2393–2398 (2007)
25. A. Kossoy, Y. Feldman, R. Korobko, E. Wachtel, I. Lubomirsky, J. Maier, Adv. Funct. Mater. **19**, 634–641 (2009)